ADVANCED FUNCTIONAL MATERIALS

DOI: 10.1002/adfm.200600637

The Effect of Nanoscale Confinement on the Collective Electron Transport Behavior in Au Nanoparticles Self-Assembled in a Nanostructured Polystyrene-*block*-poly(4-vinylpyridine) Diblock Copolymer Ultra-thin Film**

By *Chung-Ping Li*, *Chia-Hao Wu*, *Kung-Hwa Wei*,* *Jeng-Tzong Sheu*, *Jung Y. Huang*, *U-Ser Jeng*, and *Keng S. Liang*

This study involves the collective electron transport behavior of sequestered Au nanoparticles in a nanostructured polystyrene-*block*-poly(4-vinylpyridine). The monolayer thin films (ca. 30 nm) consisting of Au nanoparticles self-assembled in the 30-nm spherical poly(4-vinylpyridine) domains of an polystyrene-*block*-poly(4-vinylpyridine) diblock copolymer were prepared. From the current-voltage characteristics of these thin films, the collective electron transport behavior of Au nanoparticles sequestered in the spherical poly(4-vinylpyridine) nanodomains was found to be dictated by Coulomb blockade and was quasi one-dimensional, as opposed to the three-dimensional behavior displayed by Au nanoparticles that had been dispersed randomly in homo-poly(4-vinylpyridine). The threshold voltage of these composite increased linearly upon increasing the inter-nanoparticle distance. The electron tunneling rate constant in the case of Au nanoparticles confined in poly(4-vinylpyridine) nanodomains is eight times larger than that in the randomly distributed case and it increases upon increasing the amount of Au nanoparticles. This phenomenon indicates that manipulating the spatial arrangement of metal nanoparticles by diblock copolymer can potentially create electronic devices with higher performance.

1. Introduction

Metal nanoparticles (NPs) that have diameters in the range of 1–10 nm are the subject of much current research interest because the optical, electronic, and chemical properties of these materials, such as their single charge tunneling and plasmon resonances, are size-dependent.[1–3] As a result, such NPs are being investigated for use in various applications, including memory cells,[4] single-electron transistors,[5] and biological sensors.[6] In these applications, the NPs are often capped with organic ligands or are surrounded by other dielectric materials. Thus, an understanding of the collective electron transport of NPs dispersed in organic or dielectric materials is of both scientific and technological importance. A number of reports have described two- or three-dimensional electron transport in (a) ordered arrays of dodecanethiol-capped Ag and Au nanoparticles,[7,8] Au NPs/SiO_2 superlattices, organically capped Co NPs and (b) disordered arrays of granular films of Au NPs linked by alkanethiol molecules and Au/spacer/CdSe NP assemblies.[9–12] In contrast, very few reports describe one-dimensional electron transport within granular films, mainly because of the difficulties encountered when preparing such samples.

Nanostructured block copolymers that have period thicknesses between 10 and 100 nm, because of microphase separation of incompatible blocks, can be used as templates to selectively control the spatial arrangement of NPs within one of the blocks.[13–16] For example, the selective sequestration of presynthesized CdSe, CdS, and TiO_2 NPs into one block of a diblock copolymer can be performed by ensuring that strong interactions exist between that block of the copolymer and the surface ligands of the NPs.[17,18] Additionally, block copolymers can also be used as nanoreactors for the synthesis of nanomaterials. For example, quasi-regular arrays of Au clusters have

[*] Prof. K. H. Wei, C. P. Li
Department of Materials Science and Engineering
National Chiao Tung University
1001 Ta Hsueh Road, Hsinch 30050 (Taiwan ROC)
E-mail: khwei@mail.nctu.edu.tw
C. H. Wu
Institute of Electrophysics
National Chiao Tung University
1001 Ta Hsueh Road, Hsinch 30050 (Taiwan ROC)
Prof. J. T. Sheu
Institute of Nanotechnology
National Chiao Tung University
1001 Ta Hsueh Road, Hsinch 30050 (Taiwan ROC)
Prof. J. Y. Huang
Department of Electro-Optical Engineering
National Chiao Tung University
1001 Ta Hsueh Road, Hsinch 30050 (Taiwan ROC)
Dr. U. S. Jeng, Dr. K. S. Liang
National Synchrotron Radiation Research Center
101 Hsin-Ann Road, Hsinchu Science Park, Hsinchu 30077 (Taiwan ROC)

[**] The authors would like to acknowledge the Dr. Siao-Wei Yeh for TEM analysis, National Science Council, Taiwan, for funding (NSC 94-2120-M-009-001), and also Mr. Ching-Mao Huang for his help with the manuscript.

been obtained through the selective sequestration of metal ions into one block of polystyrene-*block*-polyvinylpyridine.[19]

The electron transport between semiconductor nanoparticles embedded differently in polymer remains unexplored until recently when the collective electron transport in CdSe quantum dots self-assembled in the poly(4-vinylpyridine) (P4VP) nanodomains of a polystyrene-*block*-poly(4-vinylpyridine) (PS-*b*-P4VP) diblock copolymer thin film was found to be dictated by tunneling behavior at room temperature.[18a] As opposed to semiconductor nanoparticles, which were often used because of their size-dependent optical properties, metal nanoparticles, which were mainly used as sensor materials due to their pronounced surface plasmon effect, appear to have different electron transport properties. In this present study, we prepared self-assembled thin films that consisted of Au NPs sequestered in the P4VP nanodomains of a PS-*b*-P4VP diblock copolymer. From the current-voltage (*I*–*V*) characteristics of these thin films at low temperature, we can find what dictate the collective electron transport behavior of Au NPs sequestered in the spherical P4VP nanodomains and how they behave, as opposed to the behavior displayed by Au NPs that had been dispersed randomly in homo-P4VP. Moreover, the electron tunneling rate constant in the case of Au NPs confined in P4VP nanodomains can also been determined.

2. Results and Discussion

Scheme 1 outlines our approach toward preparing a monolayer (Au NPs/P4VP)-*b*-PS thin film. First, the trioctylphosphine (TOP) ligands on the Au NPs, which were used during their synthesis, were replaced with hydrophilic pyridine ligands. Owing to the fact that we would like to place pyridine-modified Au NPs in P4VP domains, which is a minor phase, and both of them were hydrophilic; we chose pyridine as a good solvent for Au NPs and P4VP to form micelles having Au NPs/P4VP shells and PS cores. The Au NPs were distributed selectively in the P4VP phase as a result of dipole-dipole interactions. In order to fabricate periodically ordered two-dimensional structures, we then chose toluene, which is a hydrophobic and good solvent for PS but a poor one for P4VP, to form micelles — having Au NPs/P4VP cores and PS shells — in a solution that was spun into a thin film. After the pyridine ligands were removed during the annealing process, the Au NPs were instead capped by P4VP, and therefore the location of Au NPs was in the P4VP domain and their distribution was rather homogeneous. The (Au NPs/P4VP)-*b*-PS sample was obtained in bulk form. All samples in bulk state had underwent an annealing process, which is performed at 160 °C for 48 h, to avoid kinetically introduced variations during processing. The morphology of (Au NPs/P4VP)-*b*-PS samples did not change after being maintained at 60 °C for 36 h when they were observed with Transmission Electron Microscopy, indicating the systems arrested in an equilibrium state.

Figure 1a displays one-dimensional small-angle X-ray scattering patterns (SAXS) of (Au NPs/P4VP)-*b*-PS obtained using synchrotron radiation. The scattering maxima, which are denoted by the letter "i" ($i = 1$), are form factor peaks associated with scattering from the isolated spherical domains. The low angle peaks (at $q \sim 0.02$ Å^{-}) decreased as the amount of Au NPs increased because the periodicity of the P4VP spheres was slightly distorted when the Au NPs are present in the P4VP domains. The intensity of the form factor peaks increased as the amount of Au NPs increased; owing to the intensity of the form factor peaks of Au NPs increased. The form factor peaks shifted slightly to lower values of Q as the amount of incorporated Au increased, which indicates that the volume or size of the Au NPs/P4VP composite domains increased. The average diameter of the P4VP domains of pure PS-*b*-P4VP, deduced from the positions of the form factor maxima, was 26.6 nm. The average diameters, measured by their volume, for the 10, 15, 26, 33, and 48 % Au NPs in the P4VP block were 27.3, 27.8, 28.6, 29.3, and 30.2 nm, respectively, assuming that the density of P4VP and Au remained the same before and after mixing. The inset of Figure 1a lists the free volume per Au particle in a single P4VP domain (V_{free}), which is defined by the average volume of an occupied Au particle and can be estimated using Equations 1 and 2:

$$\frac{V_{Au/P4VP} - V_{P4VP}}{V_{Au}} = n \quad (1)$$

$$\frac{V_{Au/P4VP}}{n} = V_{free} \quad (2)$$

where $V_{Au/P4VP}$ is the volume of a single Au NPs/P4VP composite domain, V_{P4VP} is the volume of a single P4VP domain, V_{Au} is the volume of a Au NP, and n is the maximum number of Au NPs in a single P4VP

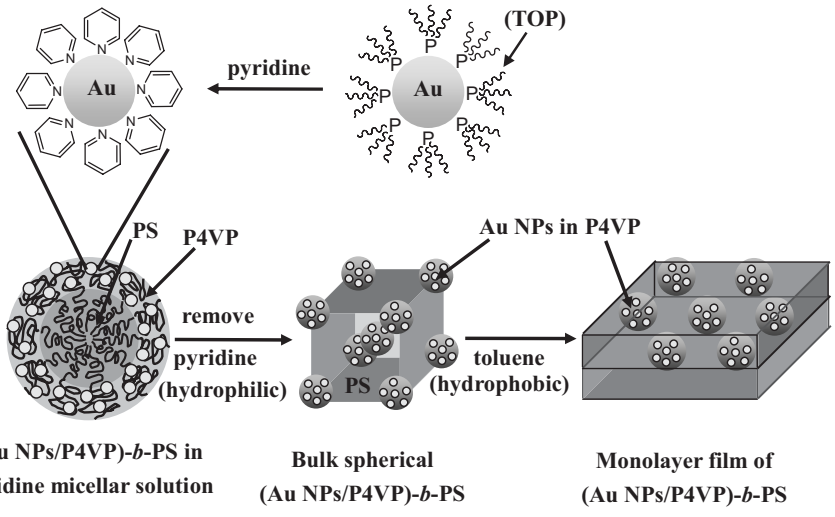

Scheme 1. Fabrication of a self assembled(Au NPs/P4VP)-*b*-PS thin film through the selective incorporation of dispersed presynthesized Au NPs into P4VP domains.

ADVANCED FUNCTIONAL MATERIALS

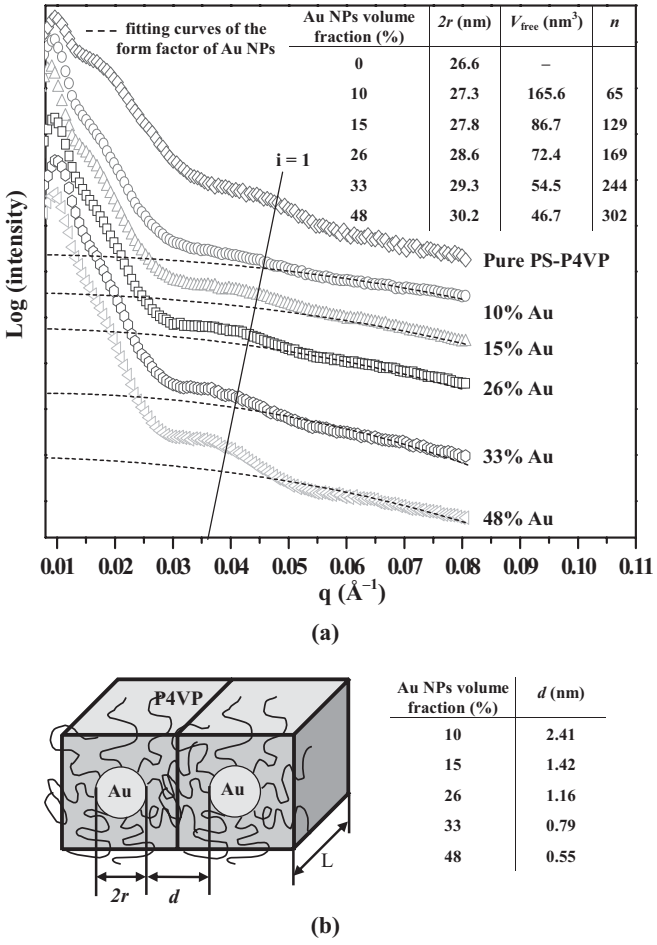

Figure 1. a) Small-angle X-ray scattering of bulk (Au NPs/P4VP)-b-PS nanocomposites having various contents of Au NPs. b) Schematic representation of the cubic lattice model for the free volume per Au nanoparticle in a single P4VP domain

domain. From analyses of the small-angle X-ray scattering peaks (as shown in Fig. 1a), we estimated that the maximum number of Au NPs sequestered within the P4VP nanodomains were ca. 65, 129, 169, 244, and 302 for the 10, 15, 26, 33, and 48 % Au NPs, respectively. The edge-to-edge interparticle distance (d) can be determined by assuming a cubic lattice model for the Au NPs. The values of d were calculated using Equation 3 based on the cubic lattice model presented in Figure 1b.[20]

$$d = L - 2r = (V_{\text{free}})^{1/3} - 2r \quad (3)$$

where r is the radius of the Au NPs. The value of d decreased when the amount of Au increased, as displayed in the inset of Figure 1b.

To compare the effect that nanodomain confinement has on the Au NPs, with respect to their randomly distributed state, we prepared two samples that had the same density of NPs in P4VP: the first contained 48 % Au NPs by volume with respect to the P4VP block in a PS-*b*-P4VP diblock copolymer, and the second contained 48 % Au NPs by volume in a P4VP homopolymer. Figure 2a displays a transmission electron microscopy (TEM) image, obtained without staining, of the top view of a thin film of 48 % (Au NPs/P4VP)-*b*-PS. The dark region represents the Au NPs/P4VP composite phase (because of the higher electron density of gold). It is clear that PS-*b*-P4VP had a spherical nanostructure. The diameter of the Au NPs/P4VP sphere was ca. 30 nm, and the inter-domain distance was ca. 90 nm. Figure 2b displays an HRTEM image of a single Au NPs/P4VP nanodomain within a thin film of 48 % (Au NPs/P4VP)-*b*-PS. The Au NPs were dispersed fairly homogeneously in the P4VP nanodomain. The inset of Figure 2b reveals the HRTEM lattice image (with a lattice spacing of ca. 2.8 Å) of one of the Au NPs incorporated within a P4VP nanodomain. The average diameter of the Au NPs was ca. 3.1 nm. Figure 2c displays a cross-sectional TEM image of a 48 % (Au NPs/P4VP)-*b*-PS thin film. The dark regions at the top and bottom of this image are the Au electrodes; the circled regions are the domains of the Au NPs/P4VP composite. Figure 2d displays a cross-sectional TEM image of a 48 % Au NPs/homo-P4VP. Au NPs were randomly distributed in the P4VP thin film. The fact that Au NPs appear to disperse in P4VP nanodomain of PS-*b*-P4VP or in P4VP homopolymer rather homogeneously as determined from the top and cross-sectional views is important for our cubic lattice model calculation since we assume interparticle distance are uniform in the calculation.

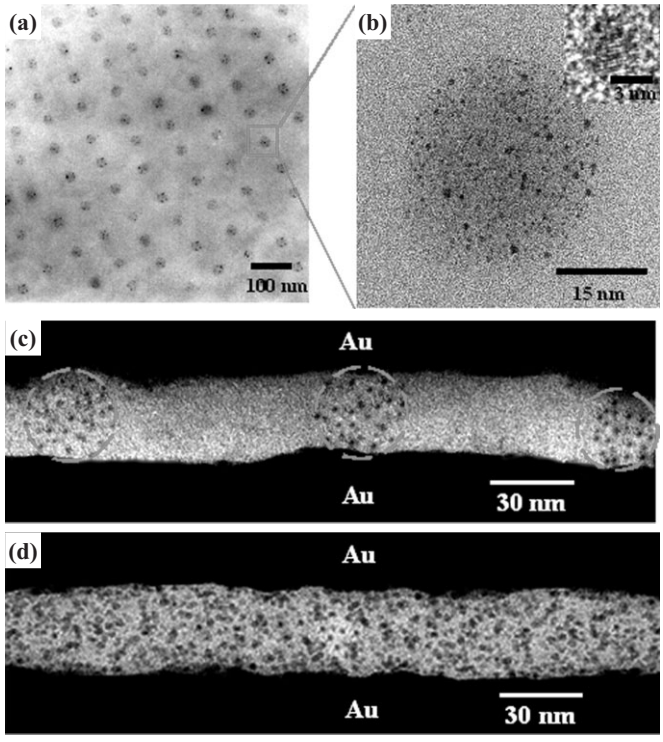

Figure 2. a) Conventional, b) high-resolution, and c) cross-sectional TEM images, obtained without staining, of a thin film of 48 % (Au NPs/P4VP)-*b*-PS. d) Cross-sectional TEM image of a thin film of 48 % Au NPs/homo-P4VP.

Figure 3a and b display the averaged *I–V* characteristics of the monolayer (Au NPs/P4VP)-*b*-PS and Au NPs/homo-P4VP thin films, both measured at temperatures within the range from 250 to 78 K. In both cases, the *I–V* curves were ohmic at 250 K, but become increasingly nonlinear upon decreasing the temperature. At 100 K and below, conduction occurred through the composite only at potentials above a minimum threshold voltage, V_T, which indicates that a collective Coulomb blockade resulted from electrical isolation of the NPs. A model for low-voltage electron transport through an array of Coulomb islands predicts thermally activated behavior for the zero-bias conductance:[7–10,21]

$$G_0 \propto \exp\left[\frac{-E_a}{k_B T}\right] \quad (4)$$

where G_0 is the zero-bias conductance, E_a is the activation energy to charge an electrically neutral nanocrystal, k_B is the Boltzmann constant, and T is the temperature. The insets to Figure 3a and b present plots of $\ln G_0$ versus $1/T$. From the slopes of the theoretical fits obtained using Equation 4, we calculated the experimental values for the activation energies (E_a) of the nanodomain-confined and randomly distributed samples to be 27 and 28 meV, respectively. The activation energy is about the same for both cases. This is because the density and the capacitance of Au NPs are the same for both cases, despite the macroscopic placement of the metal nanoparticles is different. We can also calculate E_a value theoretically since the value of E_a can be expressed as $e^2/2C$, where e is the charge of the electron and C is the total capacitance of a nanoparticle, resulting from the inter-nanoparticle capacitance, C_i, and the nanoparticle self-capacitance, C_s. Neglecting the small contribution to C from C_s, we obtained $C \approx n_0 C_i \approx n_0 2\pi\varepsilon_0\varepsilon r \ln[(r + d/2)/(d/2)]$, where ε is the dielectric constant of the surrounding P4VP matrix (ca. 3), r is the nanoparticle radius (1.5 nm), d is the interparticle distance (0.55 nm), and n_0 is the average number of nearest neighbors (assuming each nanoparticle has an average of between six to twelve nearest neighbors).[9,22] Using the parameters of $r = 1.5$ nm and $d = 0.55$ nm, we estimated that the total capacitance (C) would be between 2.3 and 4.5 aF; therefore, we calculated the activation energy to be 35–17.5 meV ($E_a \approx e^2/2C$). Thus, the experimental values of the activation energies within both the nanodomain-confined and randomly distributed samples are in reasonable agreement with the calculated values. Figure 3c displays representative current-voltage scaling data obtained for these two samples at 78 K. The accessible current-conducting pathways are described[7–10,23] by Equation 5:

$$I \propto \left(\frac{V}{V_T} - 1\right)^{\zeta} \quad (5)$$

(for $V > V_T$), where I is the current, V is the voltage, ζ is a scaling exponent, and V_T is the threshold voltage. The scaling exponent ζ can be regarded as the dimensionality for collective electron transport for arrays of dots as modeled in a previous study.[23] We obtained power-law scalings (ζ) of 1.31 for the nanodomain-confined sample and 2.84 for the randomly distributed sample. These results indicate that quasi-one-dimensional collective electron transport occurs for the nanodomain-confined Au NPs and that quasi-three-dimensional collective electron transport occurs for the randomly distributed Au NPs.

Figure 4 presents a plot of V_T versus d for nanodomain-confined and randomly distributed samples having various Au NP contents. The values of V_T of the Au NPs in the P4VP domains

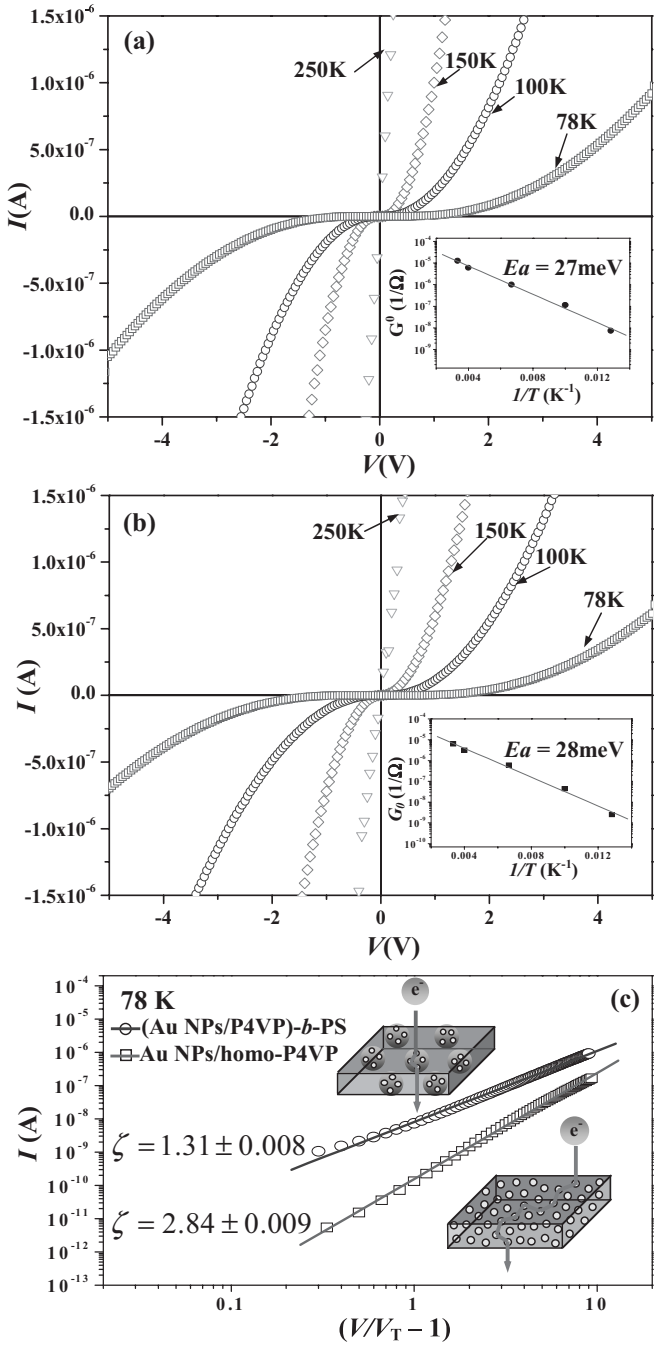

Figure 3. *I–V* curves of a) 48% (Au NPs/P4VP)-*b*-PS and b) Au NPs/homo-P4VP thin films measured at temperatures between 250 and 78 K. c) Scaling behavior of the *I–V* curves of 48% (Au NPs/P4VP)-*b*-PS and Au NPs/homo-P4VP at 78 K.

ADVANCED FUNCTIONAL MATERIALS

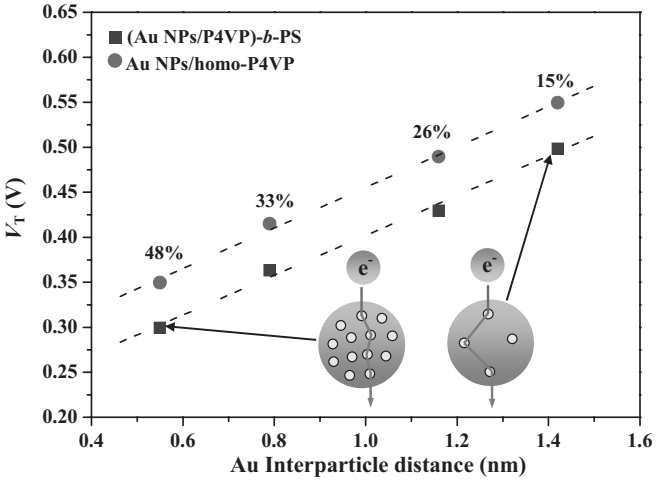

Figure 4. Plots of V_T versus d for the 48 % (Au NPs/P4VP)-*b*-PS and Au NPs/homo-P4VP samples having various contents of Au NPs.

of PS-*b*-P4VP were ca. 14 % smaller than those of the Au NPs in the homo-P4VP. In both cases, the values of V_T of these composites increased linearly upon increasing the interparticle distance because the resistance of collective electron transport increases with respect to the interparticle distance.[23]

Insets of Figures 5 and 6 display the *I–V* characteristics, measured at 78 K, of monolayered (Au NPs/P4VP)-*b*-PS and Au NPs/homo-P4VP thin films, respectively, having various contents of Au. Details of the fitting and determination of the threshold voltages and scaling exponents are provided in the Table 1. Figures 5 and 6 display representative *I–V* scaling data, recorded at 78 K, for (Au NPs/P4VP)-*b*-PS and Au NPs/homo-P4VP thin films having various contents of Au. The data in Figure 5 provide power-law scalings, ζ, for the 15, 26, 33, and 48 % Au NPs of 1.42, 1.39, 1.32, and 1.31, respectively. The pathway for electron transport should increase with the dimensionality of the space in which Au NPs occupied (indirectly the number of Au NPs) in fixed interparticle distance cases as the simulation predicted.[23] In the present case, as the number of Au NPs increase, the interparticle distance becomes shorter, and electron will more likely find a closest neighboring Au nanoparticle to tunnel through. As the number of Au NPs in a P4VP domain increase, there are more Au NPs aligning along straight lines between two planar electrodes, leading to lower power-law scalings. Therefore, the scaling reduces as the concentration of Au NPs increases. These values indicate that the effect of nanodomain confinement for quasi-one-dimensional collective electron transport for Au NPs in a nanodomain decreases when the number of Au NPs decreases. The data in Figure 6 provide power-law scalings, ζ, for the 15, 26, 33, and 48 % Au NPs of 2.89, 2.89, 2.87, and 2.84, respectively. These values indicate that the dimensionality for collective electron transport in the randomly distributed sample is independent of the number of Au NPs; i.e., quasi-three-dimensional collective electron transport occurs for the randomly distributed Au NPs.

Figure 7a displays the averaged current–voltage (*I–V*) curves of (Au NPs/P4VP)-*b*-PS thin films having various contents of Au NPs derived from the measurement of a sandwiched device at 300 K, in which a Au-coated Si wafer as the bottom electrode and Au film as the top electrode. The current must flow through Au NPs/P4VP nanodomain, owing to a much higher resistance of PS phase. The current density of a single Au NPs/P4VP nanodomain can therefore be calculated from the density of Au NPs/P4VP nanodomain in PS phase by using the following parameters, where the area of top Au electrode is 1.96×10^{-5} cm^2; the density of Au NPs/P4VP nanodomain in PS phase is 3.1×10^{11} cm^{-2} as obtained from conventional TEM image. The number of Au NPs/P4VP nanodomains under the Au electrode, N, is a product of the area of Au electrode and the density of Au NPs/P4VP nanodomains, which is about 6×10^6. We calculated the conductivity value of an Au NPs/P4VP nanodomain using Equation 6:

$$\sigma = \frac{1}{R} \times \frac{L}{N \cdot A_1} \tag{6}$$

where R is the resistance, L is the thickness between two electrodes, and A_1 is the area of a Au NPs/P4VP nanodomainan. Figure 7b displays the averaged current-voltage (*I–V*) curves of Au NPs/homo-P4VP thin films having various contents of Au NPs measured at

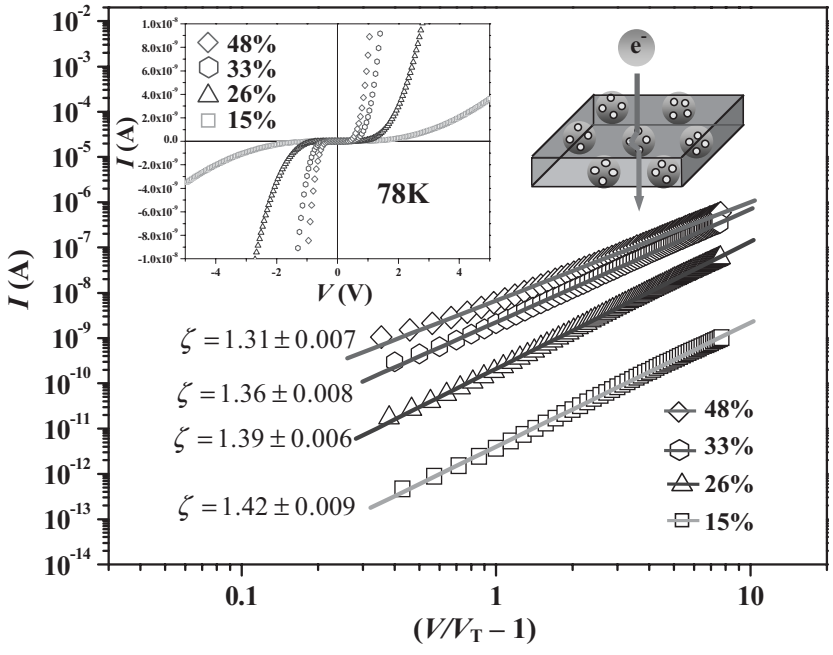

Figure 5. Scaling behavior of the *I–V* curves of (Au NPs/P4VP)-*b*-PS having various contents of Au NPs at 78 K. Inset: *I–V* Curves, measured at 78 K, of (Au NPs/P4VP)-*b*-PS thin films having various contents of Au NPs.

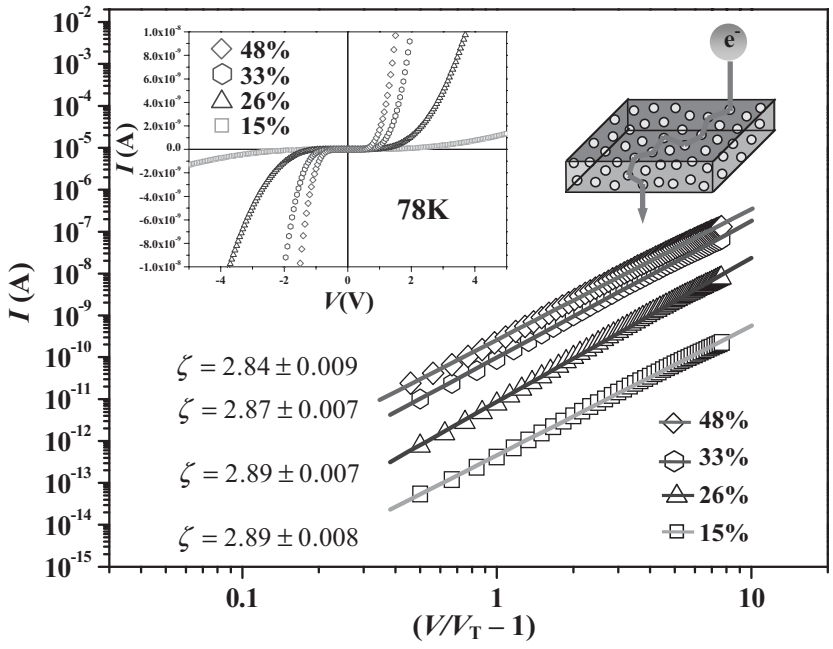

Figure 6. Scaling behavior of the *I–V* curves of Au NPs/homo-P4VP having various contents of Au NPs at 78 K. Inset: *I–V* Curves, measured at 78 K, of Au NPs/homo-P4VP thin films having various contents of Au NPs.

Table 1. Parameters of the fitting of *I–V* curves, measured at 78 K, for (Au NPs/P4VP)-*b*-PS and Au NPs/P4VP thin films having various contents of Au NPs, and determination of the threshold voltages and scaling exponents.

(Au NPs/P4VP)-b-PS $I = I_0(V/V_T - 1)^{\zeta}$				
	48%	33%	26%	15%
I_0	$(2.32 \pm 0.55) \times 10^{-9}$	$(1.81 \pm 0.45) \times 10^{-9}$	$(7.82 \pm 0.85) \times 10^{-10}$	$(7.07 \pm 0.88) \times 10^{-10}$
V_T	0.299 ± 0.006	0.363 ± 0.007	0.429 ± 0.006	0.498 ± 0.007
ζ	1.312 ± 0.007	1.362 ± 0.008	1.395 ± 0.006	1.420 ± 0.009

Au NPs/P4VP $I = I_0(V/V_T - 1)^{\zeta}$				
	48%	33%	26%	15%
I_0	$(4.38 \pm 0.67) \times 10^{-9}$	$(3.17 \pm 0.50) \times 10^{-9}$	$(1.30 \pm 0.39) \times 10^{-10}$	$(9.94 \pm 0.84) \times 10^{-10}$
V_T	0.349 ± 0.005	0.415 ± 0.006	0.489 ± 0.007	0.549 ± 0.007
ζ	2.846 ± 0.009	2.870 ± 0.007	2.893 ± 0.007	2.895 ± 0.008

300 K. We calculated the conductivity value of Au NPs/homo-P4VP thin films using Equation 7:

$$\sigma = \frac{1}{R} \times \frac{L}{A_2} \tag{7}$$

where R is the resistance, L is the thickness between two electrodes, and A_2 is the contact area of the electrode. Furthermore, the first-order electron tunneling rate constant (k_{ET}) can be estimated from the conductivity by assuming a cubic-lattice model described[24,25] by Equation 8:

$$k_{ET}(s^{-1}) = \frac{6RT\sigma}{F_a^2 \delta_c^2 C} \tag{8}$$

where R is the gas constant, T is the temperature, σ is the conductivity, F_a is the Faraday constant, δ_c is the average center-to-center interparticle distance ($\delta_c = \delta_e + 30$ Å), and C is the concentration of Au NPs in the P4VP domain (mol cm^{-3}). Table 2 shows the conductivity and electron tunneling rate constant, obtained at room temperature, for nanodomain confined and randomly distributed Au NPs in P4VP domain. In the nanodomain confined case, the current was assumed to flow through Au NPs/P4VP nanodomain, owing to a much higher resistance of PS phase. In both the nanodomain confined and randomly distributed cases, the conductivity (σ) and electron tunneling constant (k_{ET}) increase as the amount of Au NPs increased, owing to the fact that the distance between Au NPs decreased at higher Au NPs densities. Both the electron tunneling rate constant and electrical conductivity for the nanodomain confined case, which has quasi-one-dimensional collective electron transport, is about eight times larger than that of the randomly distributed case, which has quasi-three-dimensional collective electron transport.

3. Conclusion

We have demonstrated that the collective electron transport behavior between Au NPs confined within P4VP nanodomains is quasi one-dimensional, as opposed to the three-dimensional behavior displayed by Au NPs in homo-P4VP. The threshold voltage of these composite increased linearly upon increasing the inter-nanoparticle distance for both the nanodomain-confined and randomly distributed samples. The electron tunneling rate constant in the case of Au NPs confined in P4VP nanodomains is much larger than that in the randomly distributed case, and it increases upon increasing the amount of Au NPs.

Table 2. Conductivity (σ) and electron tunneling rate constant (k_{ET}) for a single P4VP domain of nanodomain-confined and randomly distributed Au NPs.

vol% of Au in P4VP	σ [Ω^{-1}cm^{-1}] × 10^7		k_{ET} [s^{-1}] × 10^{-2}	
	(Au/P4VP)-*b*-PS (nanodomain confined)	Au/P4VP (randomly distributed)	(Au/P4VP)-*b*-PS (nanodomain confined)	Au/P4VP (randomly distributed)
10	0.09	0.01	0.8	0.09
15	0.32	0.03	2.1	0.2
26	4.6	0.5	19.5	2.1
33	43.2	4.7	161.5	17.5
48	81.2	9.1	258.1	29.1

ADVANCED FUNCTIONAL MATERIALS

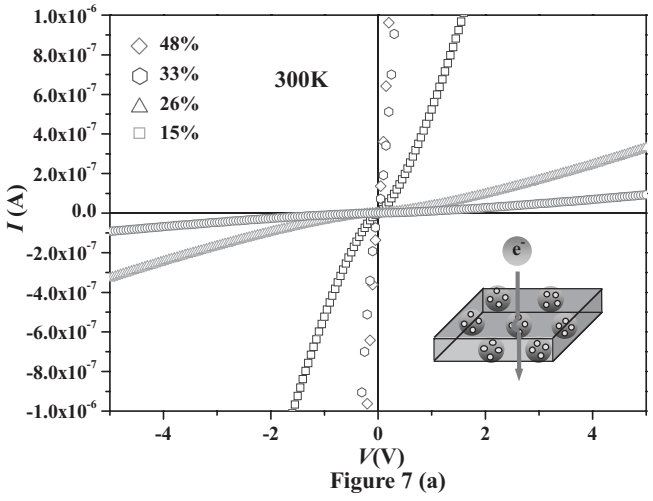

Figure 7 (a)

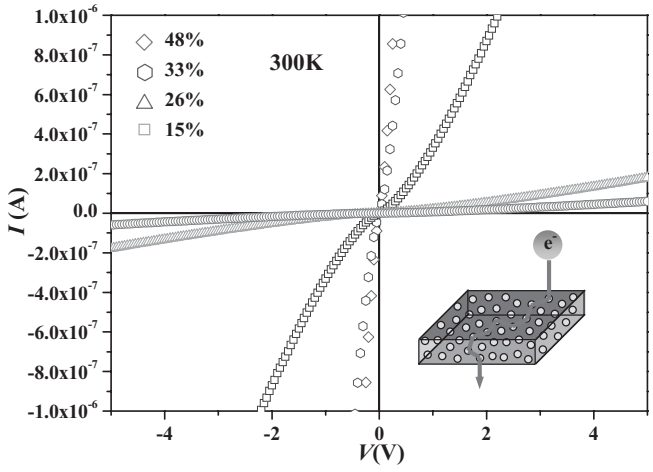

Figure 7. *I–V* Curves, measured at 300 K, of a) (Au NPs/P4VP)-*b*-PS and b) Au NPs/homo-P4VP thin films having various contents of Au NPs.

4. Experimental

Materials: The PS-*b*-P4VP diblock copolymer and the P4VP homopolymer were purchased from Polymer Source, Inc. The polydispersity index (M_w/M_n) of PS-*b*-P4VP was 1.07; the molecular weights (M_n) of the PS and P4VP blocks were 557 000 and 75 000 g mol^{-1}, respectively. Hydrogen tetrachloroaurate(III) trihydrate ($HAuCl_4 \cdot 3H_2O$), tri-*n*-octylammonium bromide (TOAB, 99 %), and sodium borohydride ($NaBH_4$, 99 %) were obtained from Acros. Trioctylphosphine (TOP, 90 %) were purchased from Aldrich. Toluene (99 %, TEDIA USA), hexane (99 %, TEDIA USA), methyl alcohol (MeOH, 99 %, TEDIA USA), and pyridine (99 %, Showa) were obtained from commercial sources.

Synthesis of Au/TOP NPs: Au/TOP NPs were synthesized using a modification of a procedure reported previously [26]. First, $HAuCl_4 \cdot 3H_2O$ (0.24 g, 0.616 mmol) was dissolved in deionized water (6.25 mL) in a 50-mL three-neck flask. This solution was added to a mixture of TOAB (0.39 g, 0.711 mmol) in toluene (8.125 mL) and stirred vigorously. Once all of the color has transferred from the aqueous layer into the organic phase, a solution of TOP (0.20 mL, 0.43 mmol) in toluene (2 mL) was injected into the reaction mixture. The organic phase turned bright red; neat TOP was then slowly added dropwise until the mixture turned a milky white color. A solution of $NaBH_4$ (88.0 mg, 2.33 mmol) in deionized water (5 mL) was then added to the mixture at a nominal rate of 7 mL h^{-1} using a syringe pump. Upon addition, the organic phase immediately darkened, progressively turning a deeper brown/black color. After the complete addition of $NaBH_4$, the reaction mixture was stirred for 30 min. The nanoparticles were collected as a powder through size-selective precipitation with methanol and then they were re-dispersed in toluene. From an analysis of over 300 Au NPs and repeated measurements on multiple samples, it indicate an average Au NP size of 3 nm diameter with standard size deviation of $\sigma \sim 13$ %.

Preparation of Au/Pyridine NPs: The Au/TOP NPs powder (30 mg) was dissolved in pyridine (5 mL) and then stirred at 65 °C for 6 h. Hexane (30 mL) was added to reprecipitate the Au NPs. The suspension was centrifuged and then the powder was collected and redissolved in pyridine.

Preparation of Bulk (Au NPs/P4VP)-b-PS: PS-*b*-P4VP (0.05 g) was added to pyridine (1 mL). Samples of 10, 15, 26, 33, and 48 % Au/pyridine (percentages with respect to the volume fraction of P4VP block) were mixed in the PS-*b*-P4VP/pyridine polymerization solution. These mixtures were dried slowly under vacuum at 50 °C and then maintained at 160 °C for 48 h to obtain the bulk (Au NPs/P4VP)-*b*-PS composites.

Preparation of Thin Films of (Au NPs/P4VP)-b-PS: Micellar solutions (0.5 wt %) of (Au NPs/P4VP)-*b*-PS were prepared by dissolving bulk (Au NPs/P4VP)-*b*-PS in toluene. The micellar solutions were spin-coated at 5000 rpm for 60 s onto carbon-coated silicon wafers [for transmission electron microscopy (TEM)] and Au-coated wafers [for current–voltage (*I–V*) curves measurements]. The sample of Au NPs distributed in the P4VP homopolymer was prepared under the same conditions used to prepare (Au NPs/P4VP)-*b*-PS, including the amount of Au in P4VP and the thickness of the thin Au NPs/homo-P4VP film.

Preparation of the Samples for Cross-Sectional TEM Images: A micellar solution of 48 % (Au NPs/P4VP)-*b*-PS in toluene was spin-coated at 5000 rpm for 60 s onto a Au-coated polyethersulfone substrate; a layer of Au (200 nm) was then vacuum-deposited as the top electrode. The sandwiched sample was placed into an epoxy capsule, which was cured at 70 °C for 48 h in a vacuum oven. The cured epoxy samples were microtomed using a Leica Ultracut Uct into ca. 50-nm-thick slices.

Characterization: TEM images were obtained using a JOEL-2010 transmission electron microscope. The thin film sample for TEM was obtained after using 1 % HF to remove the film from the carbon-coated silicon wafer. The current-voltage (*I–V*) characteristics of the thin film device of (Au NPs/P4VP)-*b*-PS were kept in a vacuum chamber in the dark and measured using a Hewlett-Packard 4156B instrument with Helium cooling system. Using a base pressure below 1×10^{-6} Torr, a layer of Au (100 nm) was vacuum-deposited as the top electrode. Small-angle X-ray scattering experiments were performed on a wiggler beamline BL-17B3 at the National Synchrotron Radiation Research Center (NSRRC), Taiwan.

Received: July 19, 2006
Revised: October 20, 2006
Published online: August 2, 2007

[1] W. J. Parak, T. Pellegrino, C. M. Micheel, D. Gerion, S. C. Williams, A. P. Alivisatos, *Nano Lett.* **2003**, *3*, 33.
[2] M. Brust, M. Walker, D. Bethell, D. J. Schiffrin, R. Whyman, *J. Chem. Soc. Chem. Commun.* **1994**, 801.
[3] C. B. Murray, C. R. Kagan, M. G. Bawendi, *Annu. Rev. Mater. Sci.* **2000**, *30*, 545.
[4] J. Ouyang, C.-W. Chu, D. Sieves, Y. Yang, *Appl. Phys. Lett.* **2005**, *86*, 123 507.
[5] U. Simon, *Adv. Mater.* **1998**, *10*, 1487.
[6] C. A. Mirkin, T. A. Taton, *Nature* **2000**, *405*, 626.
[7] C. P. Collier, R. J. Saykally, J. J. Shiang, S. E. Henrichs, J. R. Heath, *Science* **1997**, *277*, 1978.
[8] R. Parthasarathy, X. M. Lin, H. M. Jaeger, *Phys. Rev. Lett.* **2001**, *87*, 186 807.
[9] H. Fan, K. Yang, D. M. Boye, T. Sigmon, K. J. Malloy, H. Xu, G. P. López, C. J. Brinker, *Science* **2004**, *304*, 567.

[10] C. T. Black, C. B. Murray, R. L. Sandstrom, S. Sun, *Science* **2000**, *290*, 1131.
[11] a) W. P. Wuelfing, S. J. Green, J. J. Pietron, D. E. Cliffel, R. W. Murry, *J. Am. Chem. Soc.* **2000**, *122*, 11 465. b) W. P. Wuelfing, R. W. Murry, *J. Phys. Chem. B* **2002**, *106*, 3139.
[12] E. P. A. M. Bakkers, A. W. Marsman, L. W. Jenneskens, D. Vanmaekelbergh, *Angew. Chem. Int. Ed.* **2000**, *39*, 2297.
[13] a) M. J. Misner, H. Skaff, T. Emrick, T. P. Russell, *Adv. Mater.* **2003**, *15*, 221. b) Q. Zhang, S. Gupta, T. Emrick, T. P. Russell, *J. Am. Chem. Soc.* **2006**, *128*, 3898. c) Y. Lin, A. Böker, J. He, K. Sill, H. Xiang, C. Abetz, X. Li, J. Wang, T. Emrick, S. Long, Q. Wang, A. Balazs, T. P. Russell, *Nature* **2005**, *434*, 55.
[14] a) B. J. Kim, J. J. Chiu, G.-R. Yi, D. J. Pine, E. J. Kramer, *Adv. Mater.* **2005**, *17*, 2618. b) J. J. Chiu, B. J. Kim, E. J. Kramer, D. J. Pine, *J. Am. Chem. Soc.* **2005**, *127*, 5036.
[15] T. Ruotsalainen, J. Turku, P. Heikkilä, J. Roukolainen, A. Nykänen, T. Laitinen, M. Torkkeli, R. Serimaa, G. T. Brinke, A. Harlin, O. Ikkala, *Adv. Mater.* **2005**, *17*, 1048.
[16] A. M. Urbas, M. Maldovan, P. DeRege, E. L. Thomas, *Adv. Mater.* **2002**, *14*, 1850.
[17] a) S. W. Yeh, K. H. Wei, Y. S. Sun, U. S. Jeng, K. S. Liang, *Macromolecules* **2005**, *38*, 6559. b) C. C. Weng, K. H. Wei, *Chem. Mater.* **2003**, *15*, 2936.
[18] a) C. P. Li, K. H. Wei, J. Y. Huang, *Angew. Chem. Int. Ed.* **2006**, *45*, 1449. b) C. P. Li, S. W. Yeh, H. C. Chang, J. Y. Huang, K. H. Wei, *Small* **2006**, *2*, 359.
[19] a) J. P. Spatz, V. Z.-H. Chan, S. Mößmer, F.-M. Kamm, A. Plettl, P. Ziemann, M. Möller, *Adv. Mater.* **2002**, *14*, 1827. b) J. P. Spatz, S. Mossmer, C. Hartmann, M. Möller, T. Herzog, M. Krieger, H. G. Boyen, P. Ziemann, B. Kabius, *Langmuir* **2000**, *16*, 407.
[20] a) W. P. Wuelfing, S. J. Green, J. J. Pietron, D. E. Cliffel, R. W. Murry, *J. Am. Chem. Soc.* **2000**, *122*, 11 465. b) F. P. Zamborini, L. E. Smart, M. C. Leopold, R. W. Murry, *Anal. Chim. Acta* **2003**, *496*, 3.
[21] C. A. Neugebauer, M. B. Webb, *J. Appl. Phys.* **1962**, *33*, 74.
[22] In two- and three-dimensional hexagonal arrays, each nanoparticle has six and twelve nearest neighbors, respectively.
[23] A. A. Middleton, N. S. Wingreen, *Phys. Rev. Lett.* **1993**, *71*, 3198.
[24] W. P. Wuelfing, S. J. Green, J. J. Pietron, D. E. Cliffel, R. W. Murry, *J. Am. Chem. Soc.* **2000**, *122*, 11 465.
[25] F. P. Zamborini, L. E. Smart, M. C. Leopold, R. W. Murry, *Anal. Chim. Acta* **2003**, *496*, 3.
[26] J. W. Grebinski, K. L. Richter, J. Zhang, T. H. Kosel, M. Kuno, *J. Phys. Chem. B* **2004**, *108*, 9745.